Pontificia Universidad JAVERIANA Bogotá

Univ.Sci. 26(2): 193–215, 2021
doi:10.11144/Javeriana.SC26-2.saco

ORIGINAL ARTICLE

Synthesis and characterization of four N-acylhydrazones as potential O,N,O donors for Cu^{2+}: An experimental and theoretical study

María Mercedes Hincapié-Otero[1], **Andrey Joaqui-Joaqui**[1,2], **Dorian Polo-Cerón***[1]

Edited by
Juan Carlos Salcedo–Reyes
salcedo.juan@javeriana.edu.co

1. Universidad del Valle, Departamento de Química, Laboratorio de Investigación en Catálisis y Procesos, Calle 13 No 100-00, Cali, Colombia, 76001000.

2. University of Minnesota, Department of Chemistry, F-7, 139 Smith Hall, 207 Pleasant St SE Minneapolis, U.S.A., MN 55455-0431.

*dorian.polo@correounivalle.edu.co

Received: 06-07-2020
Accepted: 24-03-2021
Published online: 19-07-2021

Citation: Hincapié-Otero MM, Joaqui-Joaqui A, Polo-Cerón D. Synthesis and characterization of four N-acylhydrazones as potential O,N,O donors for Cu2+: An experimental and theoretical study, *Universitas Scientiarum*, 26(2): 193–215, 2021. doi: 10.11144/Javeriana.SC26-2.saco

Funding: Universidad del Valle –Cali, Colombia.

Electronic supplementary material: Supp. 1, Supp. 2

Abstract

N-acylhydrazones 2-(4-chlorophenyl)-N′-(2-hydroxybenzylidene)acetohydrazide, N′-(2-hydroxybenzylidene)-2-(4-methoxyphenyl)acetohydrazide, 2-(4-chlorophenyl)-N′-(2,4-dihydroxybenzylidene)-acetohydrazide, and N′-(2,4-dihydroxybenzylidene)-2-(4-methoxyphenyl)acetohydrazide were successfully synthesized by a multistep procedure. The obtained organic molecules were characterized by spectroscopic techniques (FT-IR, 1D and 2D NMR, UV-Vis) and mass spectrometry. The structure of 2-(4-chlorophenyl)-N′-(2-hydroxybenzylidene)acetohydrazide was also confirmed by X-ray diffraction. *Ab initio* computational simulations of the ligand spectra were in good agreement with experimental data and validated the hypothesis about the existence of a conformational mixture of each ligand in solution. Finally, the complexation potential of the synthesized ligands to Cu^{2+} was assessed by continuous variation experiments and FT-IR spectroscopy.

Keywords: Conformers; chelating ligands; DFT calculations; N-acylhydrazones; Schiff base; X-ray crystal structure.

1. Introduction

Currently, the chemistry of N-acylhydrazones (NAHs) and their metallic complexes has attracted increasing interest, not only because of their structural versatility, but also because they offer a wide range of applications in areas such as analytical chemistry [1], industrial chemistry [2], catalysis [3], and especially in pharmacology [4, 5].

NAHs are Schiff base-type compounds whose characteristic structural motif is the −CH=N−NH −C(=O)– linkage. They are mainly synthesized by the condensation of a hydrazide and an aldehyde or ketone in the presence of a catalytic amount of glacial acetic acid [6]. Therefore, these types of compounds can act as effective O,N,O-chelating ligands when the corresponding aldehyde or ketone is *o*-hydroxy-substituted [7]. Additionally, NAHs are highly versatile systems because they can exist as a mixture of conformers in solution and, depending on the pH, can also exhibit keto-enol tautomerism [6]. Then, from a complexation perspective, NAHs can coordinate in neutral, monoanionic or dianionic forms and produce monomeric, dimeric or even tetrameric complexes (see **Figure 1**) [8, 9].

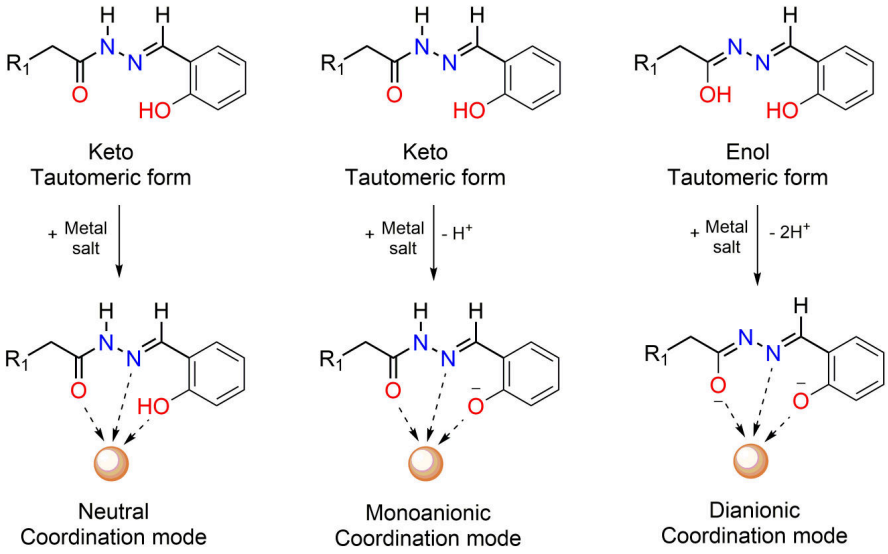

Figure 1. Salicylaldehyde-derived NAHs tautomeric forms and coordination modes.

In biological fields, copper is of interest because of its abundant presence in biological systems and its crucial role in many processes [10]. Hence, Cu^{2+} complexes derived from NAHs of salicylaldehyde and related compounds have been widely investigated. The medicinal properties of these complexes include effective DNA binding [4] and cleavage [11]; a significant bacteriostatic effect [12]; anticancer [13], antifungal [14], antioxidant [15] activities; etc.

It has been reported that salicylaldehyde benzoylhydrazone possesses mild bacteriostatic activity, while its Cu^{2+} complex is significantly more potent. Furthermore, a wide range of NAHs have been found to be cytotoxic, but again, their copper complexes have exhibited enhanced activity [16]. These findings have led to the proposal that biologically active species are indeed metallic complexes and that there is a synergy between the ligand and the metal center in the complex [17].

A discernment of the biological mechanism of action of the aforementioned complexes strongly depends on the understanding of the chemical nature of both free ligands and metallic complexes. Hence, in the present work, the synthesis and characterization of four NAHs derived from 2-hydroxibenzaldehyde and 2,4-dihydroxibenzaldehyde are described, as well as the results from theoretical calculations and dynamic ^{1}H NMR measurements, which provide some important insights into the reactivity of these types of molecules to rationalize their complexation potential to Cu^{2+}.

2. Experimental

2.1. General information

All starting reagents were purchased from commercial sources and used without further purification. All reagents were weighed and handled at room temperature. The reactions were monitored by TLC visualized by a UV lamp (254 nm or 365 nm). NMR spectra (1D and 2D) were measured on a Bruker Ultrashield 400 MHz spectrometer using DMSO-d_6 as the solvent and TMS as an internal standard. MS spectra were recorded on a Shimadzu GC-MS QP2010 spectrometer in electronic impact mode at 70 eV. UV–Vis absorption spectra were recorded on a

Thermo Scientific Evolution 220 UV-Vis spectrophotometer equipped with Single Cell Peltier System for temperature control. FT-IR spectra were recorded on a Shimadzu IRAffinity-1 infrared spectrophotometer.

2.2. Preparation of N-acylhydrazone ligands

The desired NAHs were synthesized according to the multistep procedure shown in **Scheme 1**. In the first step, a methanolic solution (10 mL) of commercially available 2-(4-chlorophenyl)acetic acid or 2-(4-methoxyphenyl)acetic acid (5 mmol) was refluxed in the presence of a catalytic amount of concentrated sulfuric acid. Then, the mixture was diluted with ether (15 mL) and washed with 3 portions of a 10 % aqueous $NaHCO_3$ solution (5 mL), and the solvent was evaporated to give methyl esters 2a and 2b as oily liquids. In the second step, the corresponding ester 2a or 2b (5 mmol) was treated with monohydrated hydrazine (10 mmol) in refluxing methanol for 3 h. After that time, the reaction mixture was concentrated, diluted with water until the cloud point and filtered. The filtered solid was washed with cold water and cold ether to finally give desired hydrazides 3a and 3b. Finally, the synthesis of the NAH ligands was based on the condensation reaction of the corresponding hydrazide with 2-hydroxybenzaldehyde to give 4a and 4b and with 2,4-dihydroxybenzaldehyde to give 5a and 5b. In both cases, the reaction mixtures dissolved in methanol were stirred at room temperature for 2 h to 5 h, and the precipitates were filtered and washed with cold methanol.

2-(4-chlorophenyl)-N′-(2-hydroxybenzylidene)acetohydrazide (4a): White solid; yield 81 %; FT-IR (ATR, cm^{-1}): 1656.9 (C=O), 1622.1 (C=N); ^{1}H NMR (400 MHz, DMSO-d_6) Major conformer δ ppm: 3.57 (s, 2H, CH_2), 6.86-6.92 (m, 2H, Ar−H), 7.23-7.39 (m, 5H, Ar−H), 7.51 (dd, 1H, Ar−H), 8.40 (s, 1H, N=CH), 11.09 (s, 1H, OH), 11.89 (s, 1H, NH). Minor conformer δ ppm: 3.96 (s, 2H, CH_2), 6.86-6.92 (m, 2H, Ar−H), 7.23-7.39 (m, 5H, Ar−H), 7.67 (dd, 1H, Ar−H), 8.30 (s, 1H, N=CH), 10.21 (s, 1H, OH), 11.36 (s, 1H, NH). Major conformer/minor

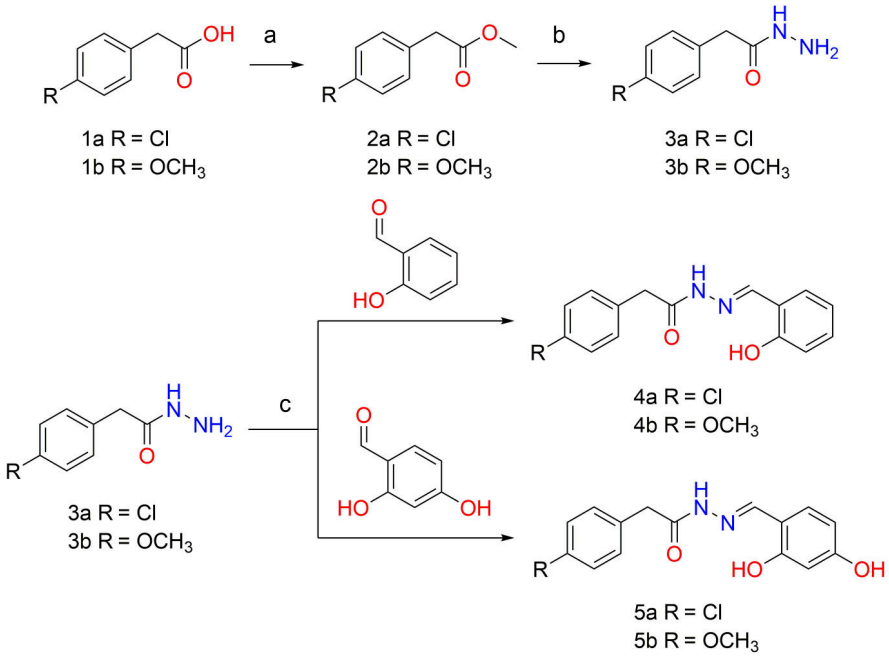

Scheme 1. Synthetic procedure for the *N*-acylhydrazone ligands. Reagents and conditions: (a) CH_3OH, H_2SO_4 (cat), reflux, 2 h; (b) N_2H_4 H_2O, CH_3OH, reflux, 3 h; (c) CH_3OH, appropriate aldehyde, CH_3COOH (cat), r.t., 2-5 h.

conformer ratio: 1:0.5; EI-MS: m/z found 288.00; formula: $C_{15}H_{13}N_2O_2Cl$. Recrystallization of the compound from ethyl acetate afforded crystals suitable for single-crystal X-ray diffraction analysis.

N′-(2-hydroxybenzylidene)-2-(4-methoxyphenyl)acetohydrazide (4b): White solid; yield 83 %; FT-IR (ATR, cm^{-1}): 1658.8 (C=O), 1610.6 (C=N); ^{1}H NMR (400 MHz, DMSO-d_6). Major conformer δ ppm: 3.46 (s, 2H, CH_2), 3.69 (s, 3H, OCH_3), 6.81-6.90 (m, 4H, Ar−H), 7.16-7.28 (m, 3H, Ar−H), 7.47 (dd, 1H, Ar−H), 8.36 (s, 1H, N=CH), 11.11 (s, 1H, OH), 11.84 (s, 1H, NH). Minor conformer δ ppm: 3.84 (s, 2H, CH_2), 3.67 (s, 3H, OCH_3), 6.81-6.90 (m, 4H, Ar−H), 7.16-7.28 (m, 3H, Ar−H), 7.63 (dd, 1H, Ar−H), 8.26 (s, 1H, N=CH), 10.25 (s, 1H, OH), 11.25 (s, 1H, NH). Major conformer/minor conformer ratio: 1:0.4; EI-MS: m/z found 284.05; formula: $C_{16}H_{16}N_2O_3$.

2-(4-chlorophenyl)-N′-(2,4-dihydroxybenzylidene)acetohydrazide (5a): Pearly light pink solid; yield 78 %; FT-IR (ATR, cm^{-1}): 1656.9 (C=O), 1626.0 (C=N); ^{1}H NMR (400 MHz, DMSO-d_6). Major conformer δ ppm: 3.52 (s, 2H, CH_2), 6.28-6.35 (m, 2H, Ar−H), 7.25-7.44 (m, 5H, Ar−H), 8.25 (s, 1H, N=CH), 10.09 (s, 1H, *p*−OH), 11.24 (s, 1H, *o*−OH), 11.68 (s, 1H, NH). Minor conformer δ ppm: 3.89 (s, 2H, CH_2), 6.28-6.35 (m, 2H, Ar−H), 7.25-7.44 (m, 4H, Ar−H), 7.43 (dd, 1H, Ar−H), 8.15 (s, 1H, N=CH), 9.95 (s, 1H, *p*−OH), 10.15 (s, 1H, *o*−OH), 11.16 (s, 1H, NH); Major conformer/minor conformer ratio: 1:0.37; EI-MS: m/z found 304.05; formula: $C_{15}H_{13}N_2O_3Cl$.

N′-(2,4-dihydroxybenzylidene)-2-(4-methoxyphenyl)acetohydrazide (5b): Pearly light pink solid; yield 77 %; FT-IR (ATR, cm^{-1}): 1631.8 (C=O), 1614.4 (C=N); ^{1}H NMR (400 MHz, DMSO-d_6). Major conformer δ ppm: 3.43 (s, 2H, CH_2), 3.69 (s, 3H, OCH_3), 6.28-6.35 (m, 2H, Ar−H), 6.82-6.87 (m, 2H, Ar−H), 7.15-7.22 (m, 2H, Ar−H), 7.25 (d, 1H, Ar−H), 8.23 (s, 1H, N=CH), (11.28 (s, 1H, *o*−OH), 11.66 (s, 1H, NH). Minor conformer δ ppm: 3.67 (s, 3H, OCH_3), 6.28-6.35 (m, 2H, Ar−H), 6.82-6.87 (m, 2H, Ar−H), 7.15-7.22 (m, 2H, Ar−H), 7.40 (d, 1H, Ar−H), 8.12 (s, 1H, N=CH), 11.08 (s, 1H, NH); Major conformer/minor conformer ratio: 1:0.3; EI-MS: m/z found 300.10; formula: $C_{16}H_{16}N_2O_4$.

2.3. Computational details

Theoretical modeling calculations of compound 4a were performed with the aid of GaussView 6.1 [18] as the graphical interface and the Gaussian 09W [19] program for computing, employing density functional theory (DFT) with Becke's three-parameter hybrid functional, the nonlocal correlation of Lee-Yang-Parr (B3LYP) and the 6-31G(d,p) basis set.

The initial structure to determine the minimum-energy geometry at the ground state was taken from the crystallographic information file. Harmonic frequency calculations were carried out to confirm that the minimum-energy structure was achieved, *i.e.*, no imaginary frequencies. The assignment of the computed frequencies was made based on potential energy distribution (PED) analysis using the Vibrational Energy Distribution Analysis (VEDA4) [20] program. Both geometric optimization and harmonic frequency calculations were performed in the gas phase.

The electronic absorption spectrum was obtained by time-dependent density functional theory (TD-DFT) calculations based on the geometry-optimized molecular structure. Solvent effects were considered with the polarizable continuum model using the integral equation formalism variant (IEFPCM). Conformational analysis was executed by performing a potential energy surface scan (PES) calculation in which the amide dihedral angle was rotated in 36 steps of 10 degrees.

2.4. Refinement

Crystal data, data collection and refinement details are summarized in **Table 1**. For the diffraction measurements, an Xcalibur, Sapphire3 Gemini diffractometer equipped with a graphite-monochromated Enhance (Mo) X-ray source ($\lambda = 0.710\,73$ Å) was used. The structure was solved using direct methods.

CCDC 2012348 contains the supplementary crystallographic data for 4a. These data can be obtained free of charge via http://www.ccdc.cam.ac.uk/structures/ or from the Cambridge Crystallographic Data Centre, 12 Union Road, Cambridge CB2 1EZ, UK; fax: (+44) 1223-336-033; or e-mail: deposit@ccdc.cam.ac.uk.

3. Results and discussion

3.1. Synthesis

NAH ligands were synthesized according to the procedure depicted in Scheme 1. NAHs were obtained in high yields (77 % to 83 %) through nucleophilic addition of the carbonyl group of 2-hydroxybenzaldehyde or 2,4-dihydroxybenzaldehyde with the respective hydrazide in the presence of a catalytic amount of glacial acetic acid. The employed synthetic approach is notably characterized by its operational simplicity, short reaction time, favorable yield, absence of drying agents and use of an inert atmosphere.

Table 1. Experimental details from structure determination of compound 4a.

Crystal Data	
Chemical formula	C15H13N2O2Cl
Mr	288.72
Crystal system	Orthorhombic
Space group	Pbca
a, b, c (angstrom)	13.3895(2), 9.5108(2), 9.5108(2)
α, β, γ (°)	90, 90, 90
V (Å3)	2688.76
Z	8
μ(mm^{-1})	0.286
Crystal size (mm^3)	$0.53 \times 0.14 \times 0.06$
Data collection	
Tmin, Tmax	2.46, 30,47
No. of measured, independent and observed [I > 2σ(I)] reflections	25 829, 3922
Rint	0.0367
Temperature (K)	130(2)
Refinement	
R[F2 >2σ(F2)], wR(F2), S	0.0483, 0.1084, 1.055
No. of reflections	3922
No. of parameters	185
No. of restraints	0

No significant difference was observed between the yield of NAHs derived from 2-hydroxybenzaldehyde (*i.e.*, 4a and 4b) and that of NAHs derived from 2,4-dihydroxybenzaldehyde (*i.e.*, 5a and 5b). These findings suggest that the electronic properties of the phenylacetic acid substituents have no influence on the overall reactivity. Moreover, the slight variance observed between the yields of 2-hydroxibenzaldehyde- and 2,4-dihydroxybenzaldehyde-derived NAHs is more related to the purification processes, where polarity differences played an important role in the washing steps. Also, the presence of the second hydroxyl group greatly enhanced the solubility of 5a and 5b in aqueous solution compared to 4a and 4b, and this feature is relevant since the main goal is to enhance the properties of the molecules to obtain biologically active molecules. Compounds 5a and 5b can be solubilized in water upon the addition of 1 % to 2 % of methanol.

Although 2,4-dihydroxybenzaldehyde-derived NAHs 5a and 5b are new compounds, 2-hydroxybenzaldehyde-derived NAHs 4a and 4b were previously synthesized [21, 22]. However, neither the structural information obtained from spectroscopic and crystallographic analyses nor any computational studies have been reported to date. For that reason, we characterized all four NAHs by spectroscopic techniques (FT-IR, 1D and 2D NMR, and UV-Vis) and mass spectrometry (EI-MS). The structure of compound 4a was confirmed by X-ray diffraction (**Figure 2**), and according to that structure, complete vibrational, electronic, and conformational studies were performed with the aid of different techniques and computational resources. Additionally, we conducted experiments to evaluate NAHs as ligands for copper complexes. All these results provide a better understanding of the behavior and overall reactivity of these molecules.

3.2. Vibrational analysis

Since assignment of fundamental vibrational modes of relatively large polyatomic molecules is not trivial, PED % analysis has become a powerful tool to interpret vibrational spectra in terms of movements of a certain group of atoms in a normal mode. PED % analysis allows to quantitatively describe the contribution of movement of a certain group of atoms in a normal mode and to represent those movements by stretching, bending and torsions (out-of-plane) of bonds, angles, and dihedral angles of two- three- and four-atomic moieties, respectively [23, 24].

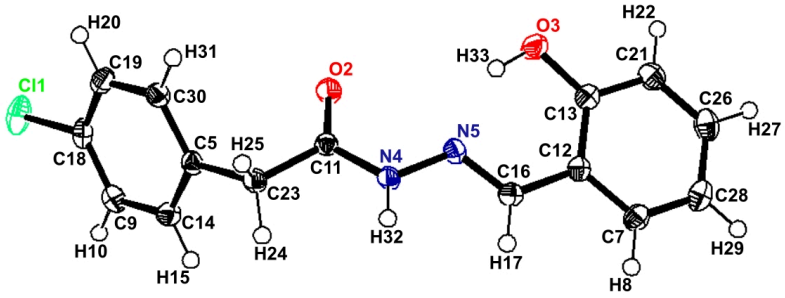

Figure 2. An ORTEP representation of the molecular structure of compound 4a obtained by X-ray diffraction with the numbering scheme and thermal ellipsoids drawn at the 50 % probability level.

Table 2. Most relevant assignments of the scaled calculated and experimental vibrational frequencies of compound 4a in terms of the potential energy distribution (PED %) analysis conducted via the VEDA4 program.

Assignment	Scaled DFT(B3LYP)		Experimental (cm^{-1})
	Calc. (cm^{-1})	**PED %**	
ν N-H	3395.7	100	3180.6
ν O-H	3283.1	99	3163.3
ν C=O	1730	85	1656.9
ν C=N	1626.1	69	1622.1

Compound 4a consists of 33 atoms and therefore exhibits 93 (3N-6) normal modes. A detailed vibrational assignment of the fundamental modes of 4a in terms of PED % is reported in Supp. 1, but **Table 2** lists the most relevant computed and experimental wavenumbers. For visual comparison, **Figure 3** presents the superposition of simulated and observed FT-IR spectra.

Vibrational frequencies derived from DFT calculations are often overestimated and, as a consequence, are commonly scaled by empirical factors. This is mainly due to the incomplete treatment of the electron correlation in the theoretical model, which also does not consider the vibrational anharmonicity of the real system. For that reason, a scaling factor of 0.9613 was used in this study to fit the calculated frequencies to the experimental frequencies [25, 26].

N−H stretching vibrations. Secondary amine N−H stretching vibrations are commonly represented by one medium-to weak intensity band that appears between 3450 cm^{-1} and 3300 cm^{-1}. However, due to hydrogen bonding, this band may be downshifted as low as 3100 cm^{-1} [27]. The computed frequency of this research appears at 3395.7 cm^{-1}, while the experimental frequency appears at 3180.6 cm^{-1}. The difference arises from the intermolecular interactions that take place in the crystal, where one molecule interacts with the other through N−H···O hydrogen bonds (**Figure 4**). Thus, the computed and experimental results are consistent with the literature results.

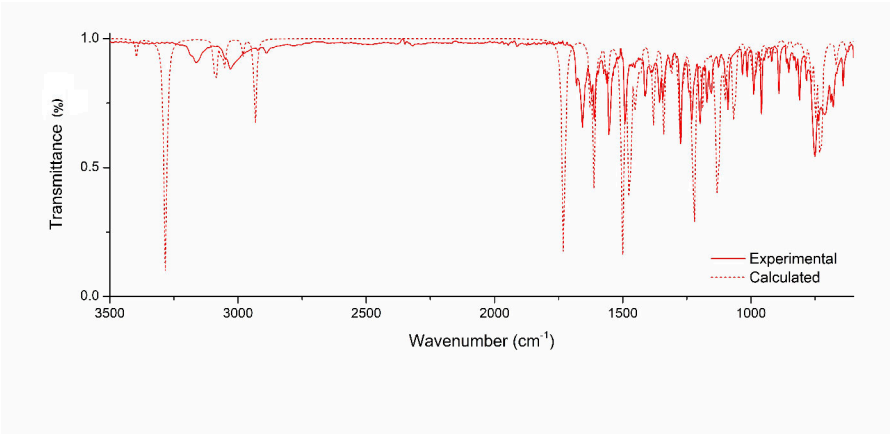

Figure 3. Superposition of observed and DFT(B3LYP)/6-31G(d,p) calculated FT-IR spectra of 4a.

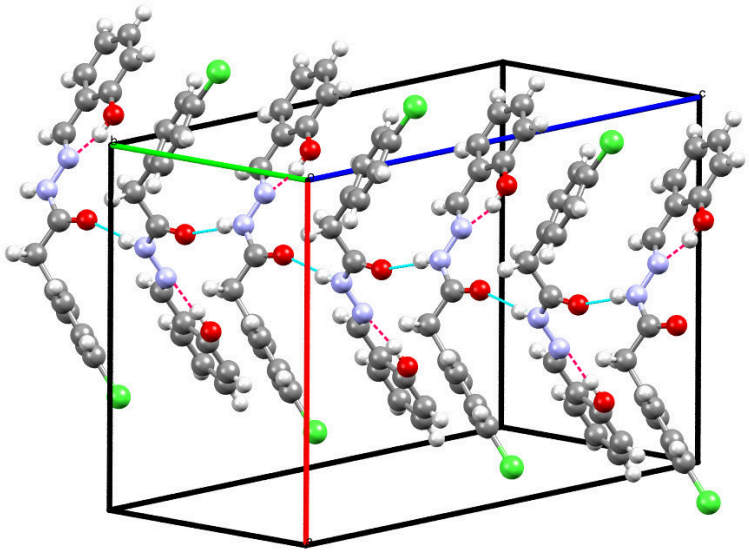

Figure 4. Intra (pink) and intermolecular (cyan) hydrogen bond interactions in 4a crystal lattice.

O−H stretching vibrations. Unassociated aromatic O−H stretching vibrations usually occur in the 3620 cm^{-1} to 3590 cm^{-1} region, while associated aromatic O−H stretching vibrations are frequently observed between 3250 cm^{-1} and 3000 cm^{-1} [27]. These vibrations are highly influenced by hydrogen bonding. In this study, computed and experimental values are in good agreement with each other and with what is reported in the literature since, according to XRD data, the molecule exhibits an O−H···N intramolecular hydrogen bond.

C=O and C=N stretching vibrations. Two factors affect the frequency of the C=O stretching vibration: the structural environment of the C=O group and the physical state of the sample. In this study, the calculated frequency was 1730 cm^{-1}, while the experimental frequency was 1656.9 cm^{-1}. The redshift is ascribable to the sum of two factors: 1. the electron-donating character of the nitrogen adjacent to the carbonyl group and 2. the intermolecular hydrogen bonds in the solid state (Figure 4). In the solid state, secondary amides usually absorb the 1680 cm^{-1} to 1630 cm^{-1} region [27]; therefore, these results are in good agreement with literature reports.

Imine bond stretching vibrations commonly appear in the 1690 cm^{-1} to 1630 cm^{-1} range [27]. Nonetheless, when the nitrogen atom is attached to extended conjugated groups, the observed band is near 1620 cm^{-1}. Consequently, computed and experimental results are consistent.

Hydrogen bonding (HB) is traditionally described as an electrostatic interaction between a proton acceptor with partial negative charge and a proton atom with a partial positive charge; however, HB is indeed a complex interplay between several phenomena, since a purely electrostatic interpretation does not justify all experimental and theoretical results, such as the redshift in hydrogen-donor group vibrational frequency [28]. Different HBs in compound 4a may be rationalized in terms of four main contributions: (i) electrostatic interactions, (ii) charge-transfer interactions, (iii) π-resonance assistance, and (iv) cooperativity.

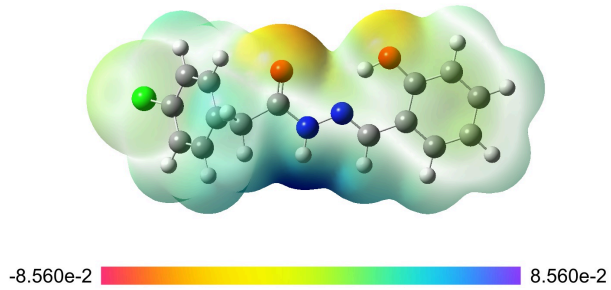

Figure 5. Molecular electronic potential (MEP) surface of compound 4a.

To prove that electrostatic interactions certainly play a crucial role in 4a amide-amide HB, the molecular electronic potential (MEP) surface was calculated as shown in **Figure 5**. MEP exhibits a negative potential (red) located over the carbonyl oxygen and a positive potential (blue) over the amino hydrogen, which means that amide moiety constitutes a permanent dipole. The main reason for this is that amide bond is characterized by an extensive charge delocalization due to $n_N \rightarrow \pi*_{C=O}$ resonance. Hence, it can be visualized as a sum of three main resonance forms, each one with a relative contribution (**Figure 6**).

Charge transfer interactions can be explained in the basis of Lewis acid-base theory, in which electronic-density transference occurs from the lone pair n_B of the Lewis base to the unfilled $\sigma_{AH}*$ orbital of the Lewis acid [28, 29]. In compound 4a the redshift in the N−H vibration frequency is therefore attributed to the population of the $\sigma_{N-H}*$ orbital upon amide-amide HB, which weakens the N−H bond due to the increment of the antibonding character and in consequence, decreases the energy required to produce the vibration.

The concept of π-resonance assisted hydrogen bond (RAHB) accounts for a particular HB strengthened by a π-conjugated system, characterized by the formation of a *quasi*-ring composed by the conjugated formally single and double bonds and the HB [30]. This model has been interpreted in several ways, and it is still objective of many investigations. One popular interpretation is based on the separation of partial charges that resonance in the π-electron system generates. The HB donor becomes more positively charged and the HB acceptor more negatively charged, being the reinforcement of the HB strength the overall result [28].

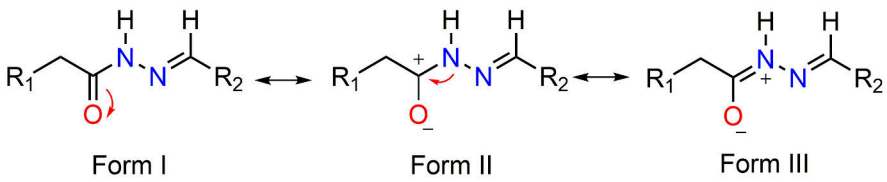

Figure 6. Amide bond resonance structures.

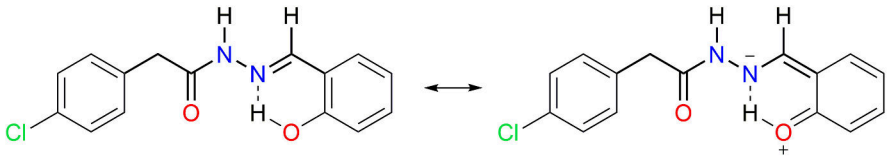

Figure 7. Resonance structures of phenol-imine moiety of compound 4a.

Besides amide resonance, the electronic density of phenol-imine moiety is also highly delocalized in compound 4a, and molecular structure can be visualized as a resonance hybrid of two canonical forms involving this moiety. Consequently, intramolecular HB between the phenol and imine nitrogen is reinforced due to the formation of a 6-membered *quasi*-ring, on which electronic density is delocalized over the π-electron system of this moiety (**Figure 7**).

Interactions like the previously discussed reinforcement between the σ and π electron system in RAHB may be dubbed as cooperative interactions, which are defined as the simultaneous occurrence of two or more interactions, being stronger than the sum of each of these interactions occurring individually [28]. A straightforward conclusion is that all different HB in compound 4a account for the spectroscopic behavior in the IR region, and clearly induce conformational preferences in the solid-state influencing packing mode in the crystal (Figure 4).

3.3. Electronic properties

Experimental UV-Vis spectrum was recorded in ethyl acetate (25 mM). To achieve a better understanding of the nature of the transitions, time-dependent density functional theory (TD-DFT) calculations were also carried out. A superposition of the experimental and calculated UV-Vis spectra of 4a is shown in **Figure 8**a.

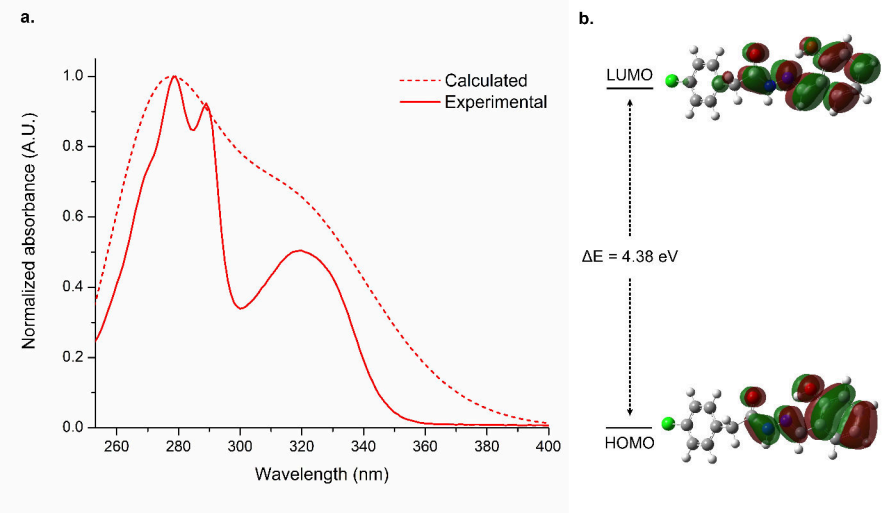

Figure 8. (a) Superposition of the observed and calculated electronic absorption spectra of 4a. (b) HOMO-LUMO transition obtained from the calculated spectrum of 4a (isovalue=0.02).

The lowest-energy band ($\lambda_{exp} = 320\,nm$) matches the TD-DFT calculations ($\lambda_{calc} = 319\,nm$). However, it should be noted that the observed and calculated higher-energy bands differ slightly. According to the literature, compounds with one saturated carbon atom between two chromophores (*e.g.*, phenyl and carbonyl groups) often exhibit fine structure spectra, especially in aprotic solvents [31], and this effect is not accurately taken into account in the calculations.

Analysis of frontier molecular orbitals may provide some insight into the reactivity of a molecule. For example, some chemical properties that can be derived from this analysis, more precisely, from the HOMO and LUMO energies, are the ionization potential (IP), electron affinity (EA), chemical hardness (η), chemical potential (μ) and electrophilicity index (ω). Chemical hardness can be expressed as $\eta = (IP - EA)/2$ [32], chemical potential can be expressed as $\mu = -(IP + EA)/2$, and the electrophilicity index can be expressed as $\omega = \mu_2/2\eta$ [33]. Koopmans' approximation [34] states that $IP = -E_{HOMO}$ and $EA = -E_{LUMO}$, and therefore, it is possible to calculate all the properties mentioned above. **Table 3** lists the calculated properties of compound 4a.

The energy bandgap between the HOMO and LUMO of compound 4a is 4.377 eV, which is a relatively large value. The larger the conjugated π orbital system, the smaller the HOMO-LUMO energy gap. As shown in Figure 8b, in compound 4a, the HOMO and LUMO are mainly localized in similar regions because the methylene group exerts conjugation disruption. According to literature reports of NAHs derived from 4-chloro and 4-bromobenzoic hydrazide and 2,4-dihydroxibenzaldehyde, in which methylene spacer is absent, HOMO and LUMO are not localized in similar regions and instead, LUMO is well distributed over the entire molecule [35, 36]. This is closely related with the calculated chemical hardness, which is the measure of the resistance of the system to reorganize the electronic cloud. Because of the disruption of the aromaticity in 4a, the computed value of this research is higher than those reported in the literature for related compounds in which methylene spacer is absent [36].

3.4. Conformational analysis

Unsymmetrical N-acylhydrazones may appear as stereoisomers (E/Z) due to the C=N bond but may also exist as conformers in solution (syn- and antiperiplanar) due to the C(=O)−N bond, as shown in **Figure 9**. The duplication of some signals in the ^{1}H and ^{13}C-NMR spectra was a common feature for all four synthesized ligands, as was the fact that the ratio between all the signal pairs appeared to remain constant, which suggests an isomeric mixture. To determine the nature of the mixture, ^{1}H-NMR at different temperatures and 2D NMR experiments (HSQC and HMBC) were carried out.

Table 3. Calculated values of HOMO and LUMO energies, energy gap and global reactivity descriptors.

Molecular property	Value (eV)
EHOMO	−5.928
ELUMO	−1.552
|EHOMO - ELUMO|	4.377
η	2.188
μ	−3.74
ω	3.196

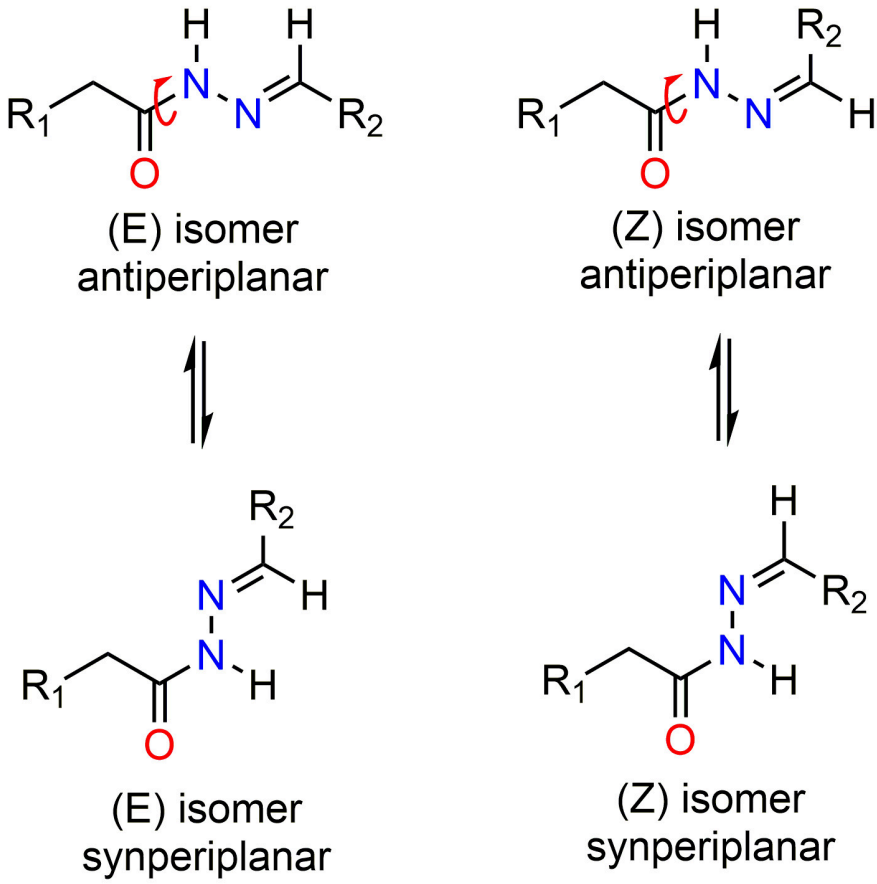

Figure 9. Isomers and conformers of *N*-acylhydrazones.

According to the literature, NAHs derived from aldehydes with an *o*-hydroxy substituent, typically exist as the (*E*) isomer because of the formation of an intramolecular hydrogen bond which stabilizes that configuration. Additionally, there are also many reports of the existence of conformers of NAHs with a spacer between the carbonyl group and the aromatic ring [37]. Therefore, NAH derived from 4-chlorophenylacetic hydrazide and acetone were synthesized to prove that the duplication of the NMR signals of the ligands respond to a mixture of two stable conformers, since (*E*/*Z*) isomerism takes place only in unsymmetrical NAHs. Indeed, all the signals in the 2-(4-chlorophenyl)-N′-(propan-2-ylidene)acetohydrazide ^{1}H-NMR spectrum (Supp. 2) were duplicated as expected, corroborating the hypothesis that all the synthesized ligands exist as a mixture of conformers in solution.

Afterward, using compound **4a** as a representative, ^{1}H-NMR experiments at different temperatures were carried out, which allowed to determine that coalescence of the duplicated signals was observed (**Figure 10**). Again, this result supported the hypothesis of two rotational isomers: the energy required to more quickly overcome the rotational barrier is reached at higher temperatures, causing rapid interconversion between the two conformers, which is not detectable on the NMR time scale [38]. Another remarkable feature derived from the experiments, which agrees with the hypothesis is that the reversibility of the interconversion was confirmed when the experimental temperature was returned to 27 °C.

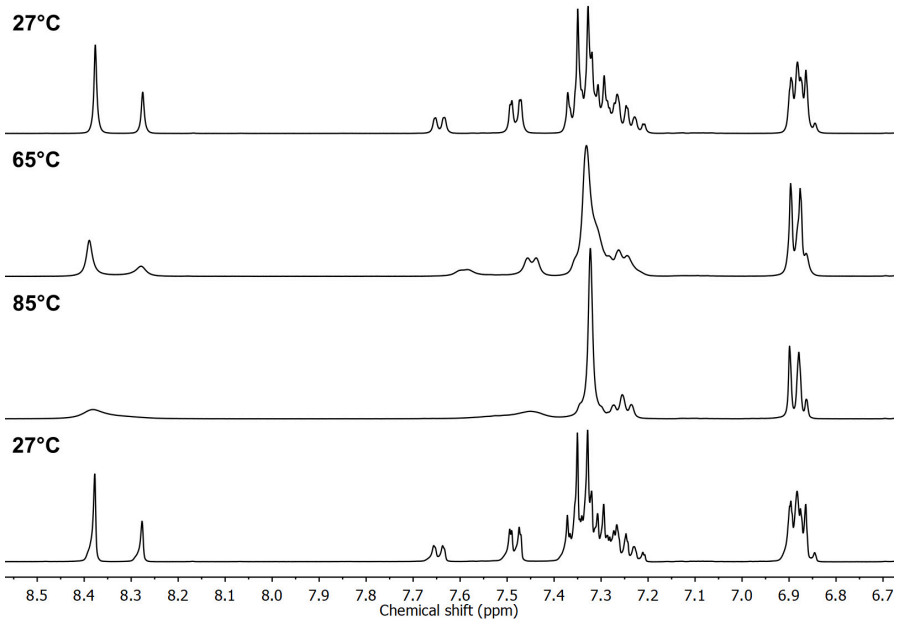

Figure 10. Variable-temperature ^{1}H NMR spectra (400 MHz, DMSO- d_6) of 4a (region from 6.7 to 8.6 ppm shown).

Amide bond rotation is detectable on the NMR time scale due to the double bond character that is a consequence of $n_N \rightarrow \pi*_{C=O}$ resonance (Figure 6). Charge delocalization along the amide bond favors a planar arrangement of this moiety; however, interconverting one rotamer into another requires a change in the nitrogen sp^2 hybridization into a pyramidal arrangement, in which the lone pair of the nitrogen is placed in an orbital with a high degree of *s* character. The disruption of the favorable interactions between N and C when this bond is twisted raises the rotational barrier; therefore, rotamers do not interconvert freely at room temperature [39]. In the transition state, C=O and N are not conjugated, and the nitrogen atom adopts a pyramidal arrangement. This is directly related to the extensive number of reports of the existence of several conformer equilibria in NAHs with an aliphatic spacer between the carbonyl group and the aromatic ring [37]. A spacer of this type disrupts the aromaticity and promotes free C−C rotation. The overall result is a poorly stabilized transition state, in which aromatic π electrons cannot interact with C^+-O^- to lower its energy.

Additionally, the energetic effects of the rotation of the amide bond were studied computationally by conducting a relaxed PES scan for the torsion around the C(=O)−N bond. The results in the gas phase (**Figure 11**) clearly showed that there are two stable conformers of the molecule, which are provided by the two local minima. The asymmetry in the plot peaks is due to the inversion of the pyramidal nitrogen in the transition state.

It is worth highlighting that according to the results shown in Figure 11, the synperiplanar (*E*)-isomer is more stable than the antiperiplanar (*E*)-isomer in the gas phase; however, in the solid state, we observed only the antiperiplanar (*E*)-isomer. This is due to the intermolecular interactions that are favored with this conformation and that are ultimately responsible for crystal growth (Figure 4).

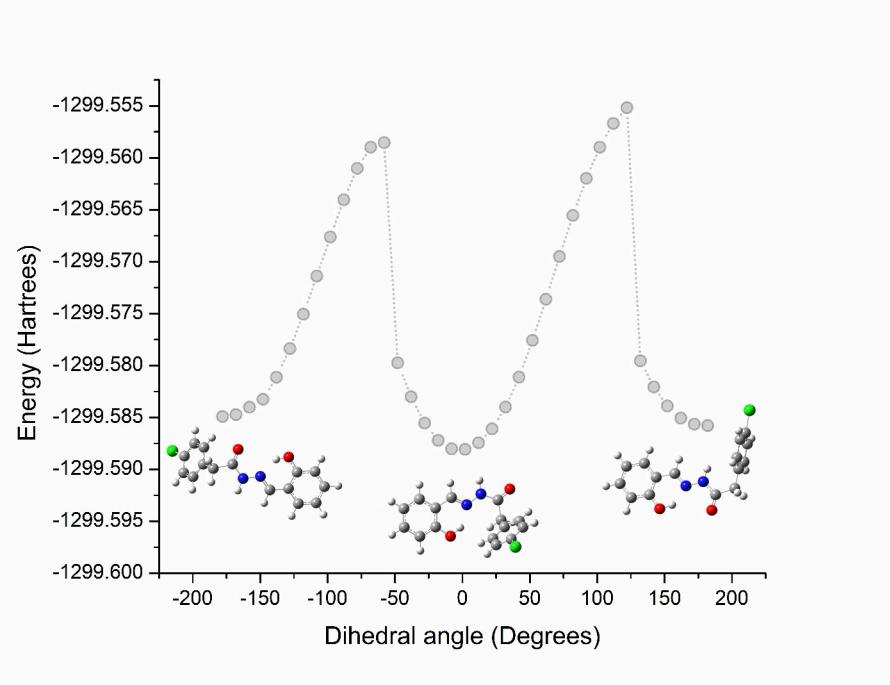

Figure 11. Potential Energy Surface (PES) scan around the amide bond of 4a.

3.5. Complexation studies

Since NAHs of salicylaldehyde and its derivatives may act as O,N,O donors, they have been widely studied for complexation of metals with potential applications in a wide range of fields *e.g.* drug development [40], catalysis [9], electronics and magnetism [41]. There have been several reports of monomeric and dimeric copper(II) complexes bearing this type of donor, acting as neutral, mono or dianionic ligands [6, 8]. Therefore, it was decided to evaluate as a first approach the complexation potential of the synthesized molecules using Job's method.

Continuous variation experiments of NAH ligand with Cu^{2+} and the resulting Job's plot (**Figure 12**) show that the ligand-Cu^{2+} complex concentration approached a maximum when the molar fraction of Cu^{2+} was 0.5, which also indicates the formation of a ligand-Cu^{2+} coordination complex with a net stoichiometry of 1:1.

To determine whether or not the NAHs acted as O,N,O donors, FT-IR spectra of 4a and the Cu-4a complex were compared (**Figure 13**). In the high-energy region, it was observed that the ν_{N-H} band shifted to 3346.5 cm^{-1}, which is closer to the computed N−H vibration value for the ligand. This is due to the loss of crystallinity in the complex, *i.e.*, the loss of the hydrogen bonding interactions responsible for the ligand's crystal growth. Additionally, the relatively narrow band at 3163.3 cm^{-1} assigned to ν_{O-H} disappeared in the spectrum of the complex, and a wide absorption band overlapping with ν_{C-H} was observed instead. This is more likely due to coordinated CH_3OH molecules.

The most remarkable features in the low-energy region of the FT-IR spectra are the shifts in the $\nu_{C=O}$ and $\nu_{C=N}$ absorption bands to lower wavenumbers. According to these results, NAHs may act as ONO donors in this kind of complexes.

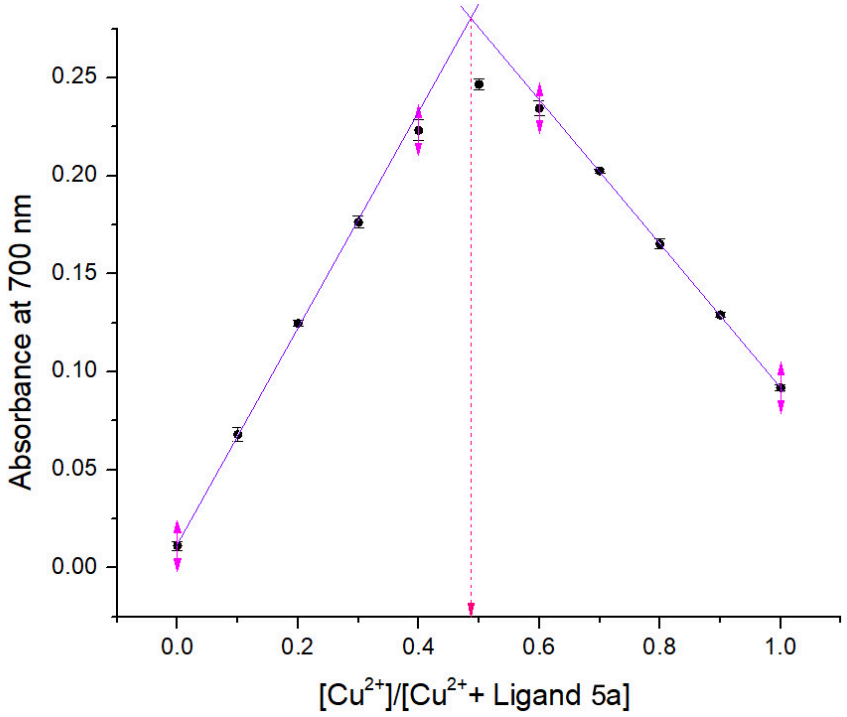

Figure 12. Job's plot resulting from the continuous variation experiment of compound 5a with Cu^{2+}.

Several reports agree that synthesis conditions strongly influence the structure of the resulting complex [8, 17]. However, the most widespread structures of Cu^{2+} complexes of salicylaldehyde-derived NAHs are binuclear complexes, in which vacant coordination sites in metal polyhedra are occupied by additional secondary ligands or solvent molecules [8]. Moreover, these complexes are characterized by their poor solubility in common solvents, similar to the complexes obtained. Therefore, in this preliminary study it is proposed that these complexes may exist as dimers (**Scheme 2**).

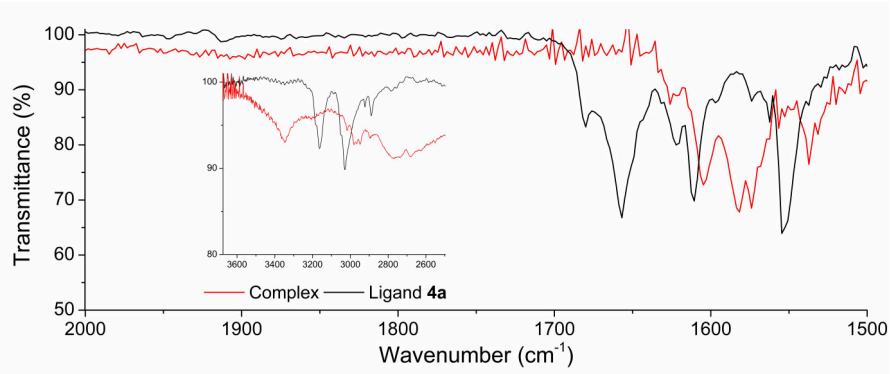

Figure 13. Superposition of relevant sections of the 4a and Cu-4a complex IR spectra.

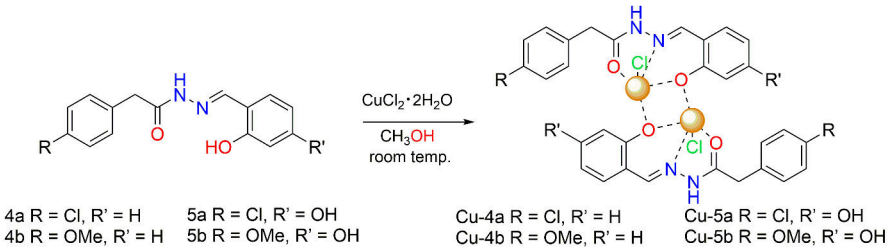

Scheme 2. Synthetic procedure for the NAH-derived copper complexes.

4. Conclusions

Four N-acylhydrazones were successfully synthesized and characterized by spectroscopic techniques, including one novel X-ray crystal structure. It is demonstrated that because of the double bond character of the amide moiety and the presence of a methylene spacer, all synthesized NAHS exist as a mixture of conformers in solution. The DFT-calculated bond lengths and angles of the solved structure were in good agreement with experimental values, allowing to simulate the FT-IR and UV-Vis spectra. Deviations between the experimental and calculated FT-IR spectra were due to intermolecular interactions that take place in the crystal lattice. Continuous variation experiments and FT-IR spectroscopy led to propose that NAHs may act as O,N,O donors for Cu^{2+} complexes that may exist as dimers in the solid state.

5. Acknowledgments

We thank the Universidad del Valle – Cali, Colombia for the equipment and reactants provided. We are grateful to Prof. Santiago Gómez-Ruiz (URJC) for his contribution to the crystallographic study.

6. Conflict of interest

The authors declare no conflict of interest.

References

[1] Chen G, Lan HH, Cai SL, Sun B, Li XL, He ZH, Zheng SR, Fan J, Liu Y, Zhang WG. Stable Hydrazone-Linked Covalent Organic Frameworks Containing O,N,O -Chelating Sites for Fe(III) Detection in Water, *ACS Applied Materials & Interfaces*, *11*(13):12830–12837, 2019.

doi: 10.1021/acsami.9b02640

[2] Singh AK, Thakur S, Pani B, Ebenso EE, Quraishi MA, Pandey AK. 2-Hydroxy- N -((Thiophene-2-Yl)Methylene)Benzohydrazide: Ultrasound-Assisted Synthesis and Corrosion Inhibition Study, *ACS Omega*, *3*(4):4695–4705, 2018.

doi: 10.1021/acsomega.8b0000

[3] Tsai YT, Chen, CY, Hsieh YJ, Tsai ML. Selective C_α Alcohol Oxidation of Lignin Substrates Featuring a β-O-4 Linkage by a Dinuclear Oxovanadium Catalyst via Two-Electron Redox Processes, *European Journal of Inorganic Chemistry, 2019*(43):4637–4646, 2019.

doi: 10.1002/ejic.201900807

[4] Ebrahimipour SY, Sheikhshoaie I, Mohamadi M, Suarez S, Baggio R, Khaleghi M, Torkzadeh-Mahani, M, Mostafavi A. Synthesis, Characterization, X-Ray Crystal Structure, DFT Calculation, DNA Binding, and Antimicrobial Assays of Two New Mixed-Ligand Copper(II) Complexes, *Spectrochimica Acta Part A: Molecular and Biomolecular Spectroscopy, 142:*410–422, 2015.

doi: 10.1016/j.saa.2015.01.088

[5] Mathew N, Sithambaresan M, Kurup MRP. Spectral Studies of Copper(II) Complexes of Tridentate Acylhydrazone Ligands with Heterocyclic Compounds as Coligands: X-Ray Crystal Structure of One Acylhydrazone Copper(II) Complex, *Spectrochimica Acta Part A: Molecular and Biomolecular Spectroscopy*, *79*(5):1154–1161, 2011.

doi: 10.1016/j.saa.2011.04.036

[6] Burgos-Lopez Y, Del Plá J, Balsa LM, León IE, Echeverría GA, Piro OE, García-Tojal J, Pis-Diez R, González-Baró AC, Parajón-Costa BS. Synthesis, Crystal Structure and Cytotoxicity Assays of a Copper(II) Nitrate Complex with a Tridentate ONO Acylhydrazone Ligand. Spectroscopic and Theoretical Studies of the Complex and Its Ligand, *Inorganica Chimica Acta*, *487*:31–40, 2019.

doi: 10.1016/j.ica.2018.11.039

[7] Aboafia SA, Elsayed SA, El-Sayed AKA, El-Hendawy AM. New Transition Metal Complexes of 2,4-Dihydroxybenzaldehyde Benzoylhydrazone Schiff Base (H2dhbh): Synthesis, Spectroscopic Characterization, DNA Binding/Cleavage and Antioxidant Activity, *Journal of Molecular Structure*, *1158*:39–50, 2018.

doi: 10.1016/j.molstruc.2018.01.008

[8] Repich HH, Orysyk SI, Orysyk VV, Zborovskii YL, Melnyk AK, Trachevskyi VV, Pekhnyo VI, Vovk MV. Influence of Synthesis Conditions on Complexation of Cu (II) with O,N,O Tridentate Hydrazone Ligand. X-Ray Diffraction and Spectroscopic Investigations, *Journal of Molecular Structure*, *1146*:222–232, 2017.

doi: 10.1016/j.molstruc.2017.05.140

[9] Sutradhar M, Kirillova MV, Guedes Da Silva, MFC, Liu CM, Pombeiro AJL. Tautomeric Effect of Hydrazone Schiff Bases in Tetranuclear Cu(II) Complexes: Magnetism and Catalytic Activity towards Mild Hydrocarboxylation of Alkanes, *Dalton Transactions 42*(47):16578–16587, 2013.

doi: 10.1039/c3dt52453a

[10] Shebl M. Coordination Behavior of New Bis(Tridentate ONO, ONS and ONN) Donor Hydrazones towards Some Transition Metal Ions: Synthesis, Spectral, Thermal, Antimicrobial and Antitumor Studies, *Journal of Molecular Structure*, *1128:*79–93, 2017.

doi: 10.1016/j.molstruc.2016.08.056

[11] Alagesan M, Bhuvanesh NSP, Dharmaraj N. Binuclear Copper Complexes: Synthesis, X-Ray Structure and Interaction Study with Nucleotide/Protein by in Vitro Biochemical and Electrochemical Analysis. *European Journal of Medicinal Chemistry*, *78*:281–293, 2014.

doi: 10.1016/j.ejmech.2014.03.043

[12] González-Baró AC, Pis-Diez R, Parajón-Costa BS, Rey NA. Spectroscopic and Theoretical Study of the O-Vanillin Hydrazone of the Mycobactericidal Drug Isoniazid. *Journal of Molecular Structure*, *1007:*95–101, 2012.

doi: 10.1016/j.molstruc.2011.10.026

[13] Fan C, Zhao J, Zhao B, Zhang S, Miao J. Novel Complex of Copper and a Salicylaldehyde Pyrazole Hydrazone Derivative Induces Apoptosis through Up-Regulating Integrin b4 in Vascular Endothelial Cells, *Chemical Research in Toxicology*, *22*(9):1517–1525, 2009.

doi: 10.1021/tx900111y

[14] Singh VP, Singh S, Singh DP. Synthesis, Characterization and Biocidal Activity of Some Transition Metal(II) Complexes with Isatin Salicylaldehyde Acyldihydrazones, *Journal of Enzyme Inhibition and Medicinal Chemistry*, *27*(3):319–329, 2012.

doi: 10.3109/14756366.2011.588228

[15] Raja DS, Bhuvanesh NSP, Natarajan K. Structure-Activity Relationship Study of Copper(II) Complexes with 2-Oxo-1,2-Dihydroquinoline-3-Carbaldehyde (4'-Methylbenzoyl) Hydrazone: Synthesis, Structures, DNA and Protein Interaction Studies, Antioxidative and Cytotoxic Activity. *Journal of Biological Inorganic Chemistry, 17*(2):223–237, 2012.

doi: 10.1007/s00775-011-0844-1

[16] Gou Y, Zhang Y, Qi J, Zhou Z, Yang F, Liang H. Enhancing the Copper(II) Complexes Cytotoxicity to Cancer Cells through Bound to Human Serum Albumin, *Journal of Inorganic Biochemistry*, *144*:47–55, 2015.

doi: 10.1016/j.jinorgbio.2014.12.012

[17] Monfared HH, Vahedpour M, Yeganeh MM, Ghorbanloo M, Mayer P, Janiak C. Concentration Dependent Tautomerism in Green $[Cu(HL^1)(L^2)]$ and Brown $[Cu(L^1)(HL^2)]$ with H_2L^1 = (E)-N -(2-Hydroxy-3-Methoxybenzylidene) Benzoylhydrazone and HL^2 = Pyridine-4-Carboxylic (Isonicotinic) Acid, *Dalton Transactions*, *40*(6):1286–1294, 2011.

doi: 10.1039/c0dt00371a

[18] Dennington R, Keith TA, Millam JM. GaussView, Version 6. Semichem Inc.: Shawnee Mission, KS 2016.

[19] Frisch MJ, Trucks GW, Schlegel HB, Scuseria GE, Robb MA, Cheeseman JR, Scalmani G, Barone V, Mennucci B, Petersson GA, Nakatsuji H, Caricato M, Li X, Hratchian HP, Izmaylov AF, Bloino J, Zheng G, Sonnenberg JL, Hada M, Ehara M, Toyota K, Fukuda R, Hasegawa J, Ishida M, Nakajima T, Honda Y, Kitao O, Nakai H, Vreven T, Montgomery Jr. JA, Peralta JE, Ogliaro F, Bearpark M, Heyd JJ, Brothers E, Kudin KN, Staroverov VN, Kobayashi R, Normand J, Raghavachari K, Rendell A, Burant JC, Iyengar SS, Tomasi J, Cossi M, Rega N, Millam JM, Klene M, Knox JE, Cross JB, Bakken V, Adamo C, Jaramillo

J, Gomperts R, Stratmann RE, Yazyev O, Austin AJ, Cammi R, Pomelli C, Ochterski JW, Martin RL, Morokuma K, Zakrzewski VG, Voth GA, Salvador P, Dannenberg JJ, Dapprich S, Daniels AD, Farkas Ö, Foresman JB, Ortiz JV, Cioslowski J, Fox DJ. Gaussian 09W. Wallingford CT 2009.

[20] Jamroz MH. Vibrational Energy Distribution Analysis VEDA 4. Warsaw.

[21] Dilanyan ÉR, Arsenyan FG, Stepanyan GM, Akopyan LG. Synthesis and Biological Activity of *N*-Acylhydrazones, *Pharmaceutical Chemistry Journal, 30*(6):368–370, 1996.

doi: 10.1007/BF02219321

[22] Desai NC, Shah MD, Bhavsar AM, Saxena AK. Synthesis and QSAR Studies of 4-Oxo-Thiazolidines and 2-Oxo-Azetidines as Potential Antibacterial Agents, *Indian Journal of Chemistry - Section B Org. Med. Chem*, *47B(07):*1135–1144, 2008.

https://doi:10.1002/chin.20084603

[23] Jamróz MH. Vibrational Energy Distribution Analysis (VEDA): Scopes and Limitations, *Spectrochimica Acta Part A: Molecular and Biomolecular Spectroscopy, 114*:220–230, 2013.

doi: 10.1016/j.saa.2013.05.096

[24] Jamróz MH, Dobrowolski JC, Brzozowski R. Vibrational Modes of 2,6-, 2,7-, and 2,3-Diisopropylnaphthalene. A DFT Study, *Journal of Molecular Structure*, *787*(1–3):172–183, 2006.

doi: 10.1016/j.molstruc.2005.10.044

[25] Wong MW. Vibrational Frequency Prediction Using Density Functional Theory. *Chemical Physics. Letters*, *256*(4–5):391–399, 1996.

doi: 10.1016/0009-2614(96)00483-6

[26] Irikura KK, Johnson RD, Kacker RN. Uncertainties in Scaling Factors for Ab Initio Vibrational Frequencies, *Journal of Physical Chemistry A*, *109*(37):8430–8437, 2005.

doi: 10.1021/jp052793n

[27] Socrates G. Infrared and Raman Characteristic Group Frequencies, John Wiley & Sons Ltd, Chichester, England 2001.

[28] Van der Lubbe SCC, Fonseca Guerra C. The Nature of Hydrogen Bonds: A Delineation of the Role of Different Energy Components on Hydrogen Bond Strengths and Lengths, *Chemistry – An Asian Journal*, *14*(16):2760-2769, 2019.

doi: 10.1002/asia.201900717

[29] Grabowski SJ. What Is the Covalency of Hydrogen Bonding? *Chemical Reviews*, 111(4):2597–2625, 2011.

doi: 10.1021/cr800346f

[30] Pareras G, Palusiak M, Duran M, Solà M, Simon S. Tuning the Strength of the Resonance-Assisted Hydrogen Bond in *o*-Hydroxybenzaldehyde by Substitution in the Aromatic Ring, *Journal of Physical Chemistry A*, *122*(8):2279–2287, 2018.

doi: 10.1021/acs.jpca.7b12066

[31] Kumler WD, Strait LA, Alpen EL. The Ultraviolet Absorption Spectra of α-Phenylcarbonyl Compounds, *Journal of the American Chemical Society*, *72*(4):1463–1466, 1950.

doi: 10.1021/ja01160a010

[32] Parr RG, Pearson RG. Absolute Hardness: Companion Parameter to Absolute Electronegativity, *Journal of the American Chemical Society, 105*(26):7512–7516, 1983.

doi: 10.1021/ja00364a005

[33] Parr RG, Szentpály LV, Liu S. Electrophilicity Index, *Journal of the American Chemical Society, 121*(9):1922–1924, 1999.

doi: 10.1021/ja983494x

[34] Koopmans T. Über Die Zuordnung von Wellenfunktionen Und Eigenwerten Zu Den Einzelnen Elektronen Eines Atoms, *Physica*, *1*(1–6):104–113, 1934.

doi: 10.1016/S0031-8914(34)90011-2

[35] Arunagiri C, Anitha AG, Subashini A, Selvakumar S. Synthesis, X-Ray Crystal Structure, Vibrational Spectroscopy, DFT Calculations, Electronic Properties and Hirshfeld Analysis of (E) -4-Bromo-N'-(2,4-Dihydroxy-Benzylidene) Benzohydrazide, *Journal of Molecular Structure, 1163:*368–378, 2018.

doi: 10.1016/j.molstruc.2018.03.023

[36] Arunagiri C, Anitha AG, Subashini A, Lokanath NK. X–Ray Crystal Structure, Hirshfeld Surface Analysis, DFT and Electronic Properties of (E)–4–Chloro–N –(2,4–Dihydroxy–Benzylidene) Benzohydrazide, *Chemical Data Collections*, *19*:100174, 2019.

doi: 10.1016/j.cdc.2018.100174

[37] Lopes AB, Miguez E, Kümmerle AE, Rumjanek VM, Fraga CAM, Barreiro EJ. Characterization of Amide Bond Conformers for a Novel Heterocyclic Template of *N*-Acylhydrazone Derivatives, *Molecules*, *18*(10):11683–11704, 2013.

doi: 10.3390/molecules181011683

[38] Huggins MT, Kesharwani T, Buttrick J, Nicholson C. Variable Temperature NMR Experiment Studying Restricted Bond Rotation. *Journal of Chemical Education,* 97(5):1425-1429, 2020.

doi: 10.1021/acs.jchemed.0c00057

[39] Stewart WE, Siddall TH. Nuclear Magnetic Resonance Studies of Amides, *Chemical Reviews*, *70*(5):517–551, 1970.

doi: 10.1021/cr60267a001

[40] Ji YW, Dai FY, Zhou B. Designing Salicylaldehyde Isonicotinoyl Hydrazones as Cu(II) Ionophores with Tunable Chelation and Release of Copper for Hitting Redox Achilles Heel of Cancer Cells, *Free Radical Biology and Medicine*, *129*:215–226, 2018.

doi: 10.1016/j.freeradbiomed.2018.09.017

[41] Costes JP, Duhayon C, Vendier L. Synthesis, Structural Characterization, and Magnetic Properties of a Copper-Gadolinium Complex Derived from a Hydroxybenzohydrazide Ligand, *Inorganic Chemistry, 53*(4):2181–2187, 2014.

doi: 10.1021/ic4027283

Síntesis y caracterización de cuatro N-acil hidrazonas como potenciales donadores de O,N,O para Cu^{2+}: un estudio teórico y experimental

Resumen: Se sintetizaron exitosamente las N-acil hidrazonas 2-(4-clorofenil)-N′-(2-hidroxi bencilideno)acetohidrazida, N′-(2-hidroxibencilideno)-2-(4-metoxifenil)acetohidrazida, 2--(4-clorofenil)-N′-(2,4-dihidroxibencilideno)acetohidrazida y N′-(2,4-dihidroxibencilideno)-2-(4-metoxifenil)acetohidrazida en un procedimiento de múltiples pasos. Las moléculas orgánicas obtenidas se caracterizaron por medio de técnicas espectroscópicas (FT-IR, RMN 1D y 2D, UV-Vis) y espectrometría de masas. La estructura de la 2-(4-clorofenil)-N′-(2-hidroxibencilideno)acetohidrazida fue confirmada además por difracción de rayos-X. Cálculos computacionales de simulación a primeros principios de los espectros del ligando concordaron bien con los datos experimentales y validaron la hipótesis acerca de la existencia de una mezcla conformacional de cada ligando en solución. Finalmente, el potencial de complejación de los ligandos sintetizados al Cu^{2+} fue determinado por experimentos de variación continua y espectroscopía FT-IR.

Palabras Clave: Confórmeros; ligandos quelantes; cálculos DFT; N-acil hidrazonas; bases de Schiff; estructura cristalina por rayos-X.

Síntese e caracterização de quatro N-acil hidrazonas como doadoras potenciais de O,N,O para Cu^{2+}: Um estudo experimental e teórico

Resumo: As N-acil hidrazonas 2-(4-clorofenil)-N′-(2-hidroxibencilideno)acetohidrazida, N′-(2-hidroxibencilideno)-2-(4-metoxifenil)acetohidrazida, 2-(4-clorofenil)-N′-(2,4-dihidroxibencilideno)acetohidrazida e N′-(2,4-dihidroxibencilideno)-2-(4-metoxifenil)acetohidrazida foram sintetizadas com sucesso mediante um procedimento de múltiplos passos. As moléculas orgânicas obtidas foram caracterizadas por técnicas espectroscópicas (FT-IR, RMN de 1D e 2D, UV-Vis) e espectrometria de massas. A estrutura da 2-(4-clorofenil)-N'-(2-hidroxibencilideno)acetohidrazida foi confirmada adicionalmente por difração de raios-X. As simulações computacionais *Ab initio* do espectro do ligante concordaram com os dados experimentais e validaram a hipótese sobre a existência de uma mistura conformacional de cada ligante em solução. Finalmente, se avaliou o potencial de complexação entre os ligantes sintetizados e Cu^{2+} por experimentos de variação contínua e FT- IR.

Palavras-chave: Confórmeros; ligantes quelantes; cálculos DFT; N-acil hidrazonas; base de Schiff; estrutura cristalina por raios-X.

María Mercedes Hincapié-Otero

She earned her bachelor's degree in Chemistry at Universidad del Valle in 2020. There, moved by her interest in metallic complexes with biological applications, she developed her undergraduate research project under the direction of Professor Dorian Polo-Cerón in the bioinorganic chemistry research group. Recently, Maria got admitted into King Abdullah University of Science and Technology as a graduate student and will pursue a degree in Bioscience.

ORCID: 0000-0001-8750-1729

Andrey Joaqui

He grew up in Cali (Colombia) where he completed his Bachelor of Science in Chemistry at Universidad del Valle, carrying out a final year research project on the synthesis of lanthanide-based coordination compounds. In 2017, he joined the chemistry department at the University of Minnesota to pursue his Ph.D. degree. His research interests include the development of metal-based antimicrobials, PET and MRI contrast agents.

ORCID: 0000-0001-7446-6004

Dorian Polo-Cerón

He gained his Ph.D. in chemistry from Rey Juan Carlos University, Spain(2008). He then undertook post-doctoral research with Professor Glen Deacon, Monash University, Australia(2009). Dorian was appointed to the academic staff of Universidad del Valle in 2010. His research interests involve many aspects of inorganic chemistry of the main group and lanthanoid elements. These compounds are relevant to areas such as catalysis, bioinorganic and medicinal chemistry.

ORCID: 0000-0002-6778-2209